Available online at www.sciencedirect.com
ScienceDirect
Trans. Nonferrous Met. Soc. China 25(2015) 2415−2421
Transactions of Nonferrous Metals Society of China
www.tnmsc.cn

Non-isothermal thermal decomposition kinetics of high iron gibbsite ore based on Popescu method

Zheng-gen LIU[1], Zheng WANG[1], Jue TANG[1], Hong-tao WANG[1], Hong-ming LONG[2]

1. School of Materials and Metallurgy, Northeastern University, Shenyang 110819, China;
2. School of Metallurgical Engineering, Anhui University of Technology, Ma'anshan 243002, China

Received 16 September 2014; accepted 15 April 2015

Abstract: The thermal decomposition kinetics of high iron gibbsite ore was investigated under non-isothermal conditions. Popescu method was applied to analyzing the thermal decomposition mechanism. The results show that the most probable thermal decomposition mechanism is the three-dimensional diffusion model of Jander equation, and the mechanism code is D3. The activation energy and pre-exponential factor for thermal decomposition of high iron gibbsite ore calculated by the Popescu method are 75.36 kJ/mol and 1.51×10^5 s^{-1}, respectively. The correctness of the obtained mechanism function is validated by the activation energy acquired by the iso-conversional method. Popescu method is a rational and reliable method for the analysis of the thermal decomposition mechanism of high iron gibbsite ore.

Key words: high iron gibbsite ore; thermal decomposition kinetics; activation energy; pre-exponential factor; Popescu method

1 Introduction

High iron gibbsite ore consists of goethite (FeOOH), gibbsite ($Al(OH)_3$), diaspore (AlOOH), and little other minerals. The high iron gibbsite ore spreads over some countries, such as China, Australia, Greece, Brazil and America. The national reserve of high iron gibbsite ore in China attains to more than 1.5 billion tons [1]. With the aim to achieve comprehensive utilization of this ore, many researches have been carried out, and several treatment processes have been presented successively, such as direct reduction−magnetic separation of the iron−alumina leaching [2−5], sintering agglomeration−blast furnace ironmaking−alumina leaching [6,7] and direct reduction−smelting separation of the iron−alumina leaching [8]. These processes have a common characteristic of ironmaking first and then alumina leaching. If the problems of high energy consumption and high cost in these processes can be solved, these processes would be able to develop well.

During the ironmaking step in these processes, the thermal decomposition of high iron gibbsite ore would be generated. The thermal decomposition kinetics of high iron gibbsite ore contributes to the development and improvement of these processes. However, the thermal decomposition mechanism of high iron gibbsite ore has not been reported. Most studies of thermal decomposition kinetics of bauxite focused on the gibbsite. ZHU et al [9] researched dehydration reaction kinetic of gibbsite with Kissinger equation. MACKENZIE et al [10] summarized the thermal decomposition of mechanically activated gibbsite. AMIRPIRAN et al [11] studied the non-isothermal dynamic model for the thermal decomposition of a gibbsite particle. And also AMIRPIRAN et al [12] developed a multi-stage, multi-reaction shrinking core model for self-inhibiting gas−solid reactions of gibbsite. However, the researches on the non-isothermal thermal decomposition kinetics of high iron gibbsite ore are quite limited.

This work focused on the non-isothermal thermal decomposition kinetics of high iron gibbsite ore. And its corresponding kinetics parameters were researched by Popescu method. This work could provide a deep insight into the thermal decomposition mechanism of high iron gibbsite ore. And also it could ensure optimal and proper control for the thermal decomposition conditions of high iron gibbsite ore, which are helpful to the efficient energy saving and prospective utilization of high iron gibbsite ore in various processes.

Foundation item: Project (51374058) supported by the National Natural Science Foundation of China
Corresponding author: Hong-ming LONG; Tel: +86-555-2311571; E-mail: yaflhm@126.com
DOI: 10.1016/S1003-6326(15)63857-2

2 Experimental

2.1 Samples preparation

The high iron gibbsite ore samples used in this investigation were obtained from Guangxi region in China. Before experiments, the samples were firstly ground to particle size less than75 μm, and then they are dried at 105 °C for 5 h.

Table 1 shows the major chemical composition of high iron gibbsite ore. It can be seen that the alumina and ferric oxide contents are 23.85% and 49.21%, respectively. The high iron gibbsite ore is a run-of-mine ore with characteristics of high iron, high silica and low A/S ratio.

Table 1 Major chemical compositions of high iron gibbsite ore (mass fraction, %)

Fe_2O_3	SiO_2	Al_2O_3	CaO	MgO	S	P	TFe
49.21	7.16	23.85	0.01	0.21	0.03	0.12	34.68

The mineral composition of high iron gibbsite ore was investigated by means of X-ray diffraction. Figure 1 shows the XRD pattern of high iron gibbsite ore analyzed by the search match software. It can be concluded that the main crystalline phases are goethite (FeOOH), gibbsite ($Al(OH)_3$), diaspore (AlOOH), hematite (Fe_2O_3), and silica (SiO_2).

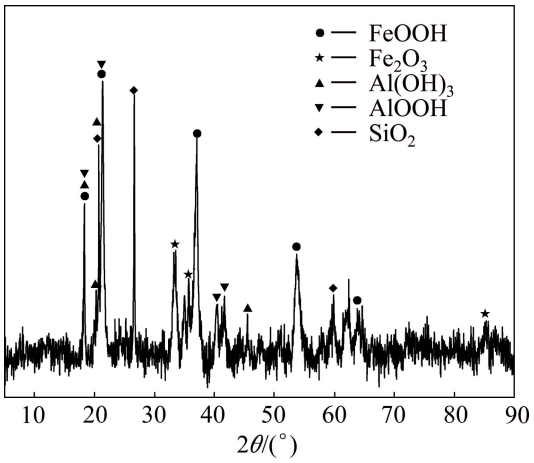

Fig. 1 XRD pattern of high iron gibbsite ore

2.2 Thermogravimetric experiments

Non-isothermal decomposition experiments were carried out using a Netzsch STA 409 C/CD in Ar atmosphere (99.99%, volume fraction). A sample of about 10 mg was taken for each run and heated from room temperature to 800 °C with a steady Ar flow (40 mL/min) maintained through the reactor tube. The samples were used at different heating rates, 5, 10, 15, 20 °C/min, respectively.

2.3 Popescu analysis method

Popescu method, as well as a variant on the Flynn−Wall−Ozawa method, was put forward by POPESCU [13] in 1996. The Popescu method is a method of multiple scanning rate. The activation energy E, the pre-exponential factor A and the mechanism functions $f(\alpha)$ were obtained by dealing with the degree of conversion at the same temperature on several TG curves at different heating rates. The main advantages of this method are that it neither includes any assumption concerning the temperature integral, nor takes the form of $k(T)$ into account, and the results have a higher precision [14]. And the method allows the activation energy to be determined as a function of the extent of conversion and/or temperature without making any assumption about the reaction model.

In general, the governing equation for kinetics analysis of solid state decomposition is as follows:

$$\frac{\mathrm{d}\alpha}{\mathrm{d}t}=k(T)f(\alpha) \tag{1}$$

where t is the time, T is the temperature, α is the extent of conversion and $k(T)$ is the temperature dependence of the rate constant.

By the usual change of the variable time into temperature, Eq. (1) becomes

$$\frac{\mathrm{d}\alpha}{\mathrm{d}T}=\frac{1}{\beta}k(T)f(\alpha) \tag{2}$$

where β=dT/dt is the heating rate.

Because in most experiments, the heating rate is kept constant, in Popescu method, the integral form of Eq. (2) is

$$\int_{\alpha_m}^{\alpha_n}\frac{\mathrm{d}x}{f(x)}=\frac{1}{\beta}\int_{T_m}^{T_n}k(y)\mathrm{d}y \tag{3}$$

where α_m and α_n are two different degrees of conversion and T_m and T_n are their corresponding temperatures. By using the notations

$$G(\alpha)_{mn}=\int_{\alpha_m}^{\alpha_n}\frac{\mathrm{d}\alpha}{f(\alpha)} \tag{4}$$

$$I(T)_{mn}=\frac{1}{\beta}\int_{T_m}^{T_n}k(T)\mathrm{d}T \tag{5}$$

$$G(\alpha)_{mn}=\frac{1}{\beta}I(T)mn \tag{6}$$

Equation (6) is actually the basis of the method for finding the most probable kinetic mechanism of the studied reaction.

It has to be assumed that over certain ranges of α and β values, the kinetics of the reaction does not change. For example, the analytical forms of $f(\alpha)$ and $k(T)$, consequently $G(\alpha)_{mn}$ and $I(T)_{mn}$, are not changed when

either α or β is varied.

On the basis of the experimental data, a pairs of α, such as (α_{m1}, α_{n1}), (α_{m2}, α_{n2}), ⋯, (α_{mi}, α_{ni}) will be determined, when $T=T_m$ and T_n, under the different heating rates β. With the help of these pairs and various functions, the values of $G(\alpha)_{mn1}$, $G(\alpha)_{mn2}$, ⋯, $G(\alpha)_{mni}$ could be computed based on Eq. (4). And for each conversation function $f(\alpha)$, the corresponding values were acquired. As the temperatures T_m and T_n are the same for all the experiments, according to Eq. (5), it follows that $I(T)_{mn}$ is constant, and from Eq. (6), a plot of the values of $G(\alpha)_{mn}$ versus $1/\beta$ will lead to a straight line with an intercept of zero if the analytical form of $f(\alpha)$ is properly selected. With the data analysis, a series of straight lines will indicate the best kinetics model by the best linear correlation coefficient.

The equations for calculating activation energy E and pre-exponential factor A are as follows:

$$\ln\left[\frac{\beta}{T_n-T_m}\right]=\ln\left[\frac{A}{G(\alpha)_{mn}}\right]-\frac{E}{RT_{\xi}} \tag{7}$$

where $T_{\xi}=(T_m+T_n)/2$. By substituting the values of (T_{m1}, T_{n1}), (T_{m2}, T_{n2}), ⋯, (T_{m5}, T_{n5}) and mechanism functions $G(\alpha)_{mn}$ into Eq. (7), the kinetic parameters of E, A and linear correlation r were obtained by the linear least squares method with $\ln[\beta/(T_n-T_m)]$ versus $1/T_{\xi}$.

3 Results and discussion

3.1 Analysis on TG−DSC curves

Figures 2−4 give the TG curves, DSC curves and conversion degree curves of high iron gibbsite ore heated at different heating rates, respectively. From Fig. 2, the TG curves of high iron gibbsite ore could be divided into three stages roughly. The segment points of each stages have some changes and hysteretic phenomenon with the increase of the heating rate. From Fig. 3, there is an obvious endothermic peak of each curve with the temperature between 250 and 290 °C. However, the endothermic peaks with the temperature between 50 and 150 °C are not remarkable. As shown in Fig. 1, the high iron gibbsite ore mainly consists of goethite (FeOOH), gibbsite($Al(OH)_3$) and diaspore(AlOOH). These hydrates would decompose when they are heated to a certain temperature. Combining the characteristic of goethite, gibbsite and diaspore with the TG−DSC curves, it could be concluded that the thermal decomposition could divide into three stages [15,16]. The first is the stage of losing absorption water (0−200 °C), and the next is dehydroxylation of gibbsite and goethite (200−300 °C), and the last is dehydroxylation of diaspore (300−500 °C). Figure 5 shows the XRD pattern of high iron gibbsite ore heated at the temperatures of 600 and 800 °C, respectively. It can be seen that there is almost no change

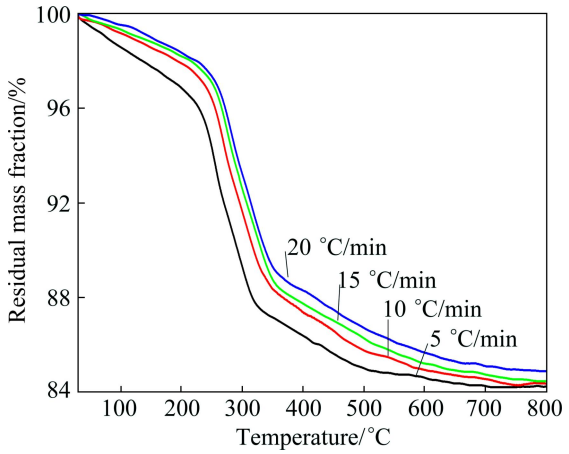

Fig. 2 TG curves of high iron gibbsite ore heated at different heating rates

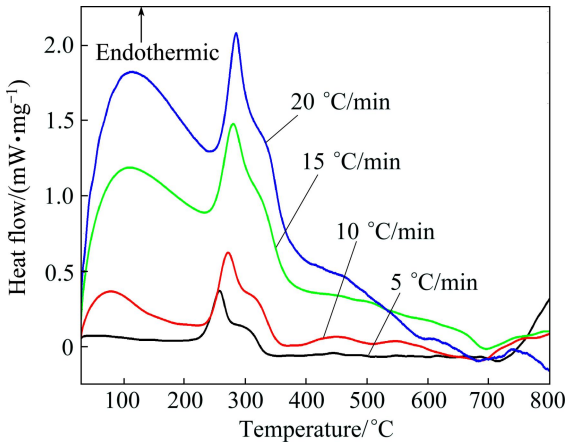

Fig. 3 DSC curves of high iron gibbsite ore heated at different heating rates

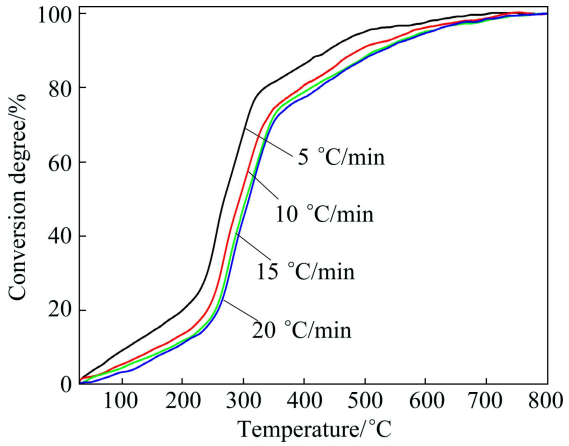

Fig. 4 Conversion degree curves of high iron gibbsite ore heated at different heating rates

of the mineral compositions of high iron gibbsite ore heated at 600 and 800 °C. Based on Figs. 2 and 5, it could be drawn that the decomposition of minerals in the samples is completed when the temperature reaches 800 °C. As the characteristic of thermal decomposition

of high iron gibbsite ore is the dehydration of goethite (FeOOH), gibbsite ($Al(OH)_3$) and diaspore (AlOOH), it is possible that the thermal decomposition kinetics of high iron gibbsite ore is calculated by the mass loss or heat flow.

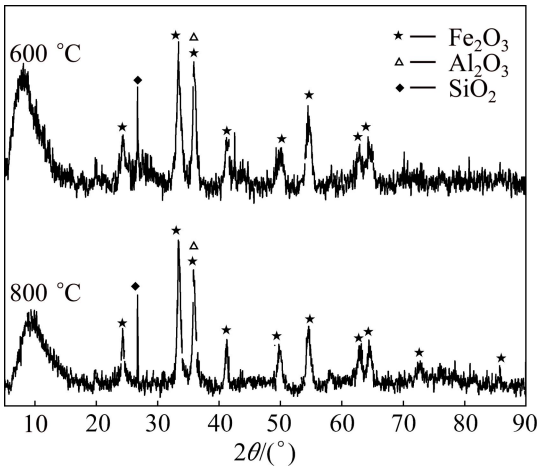

Fig. 5 XRD patterns of high iron gibbsite ore heated at 600 and 800 °C

3.2 Determination on thermal decomposition mechanism function

Forty-one kinds mechanism functions in reference were analyzed [17]. Among them, 6 kinds of diffusion model, 2 kinds of random nucleation−subsequent growth model and 2 kinds of reaction order model present a good linearity. The integral form $G(\alpha)$ and the differential form $f(\alpha)$ of these models are shown in Table 2 [18−21].

In order to determinate the thermal decomposition mechanism function of high iron gibbsite ore, as shown in Table 3, some temperatures T_m and T_n and the corresponding conversion degrees for each of them are selected. The selected temperatures are around 300 °C (573.15 K), because these temperatures could represent the relationship among conversion degrees, temperatures and heating rates at the greatest extent, so as to reduce the random error resulted from selecting thermal decomposition temperature.

By substituting the conversion degrees for each of them in Table 3 and kinetics mechanism functions in Table 2 into Eq. (4), respectively, the values of $G(\alpha)_{mn}$ at different heating rates for every conversion function are obtained. Plotting $G(\alpha)_{mn}$ versus $1/\beta$ and applying a linear fitting least squares method with an intercept of zero, the inferring schematic diagram of the most probability mechanism function is shown in Fig. 6.

The calculated linear correlation coefficients r and standard deviations r_{SD} for each kinetic mechanism functions are listed in Table 4. Liner correlation coefficients r reflect the goodness of fitting for linear logarithmic stronghold. The standard deviations r_{SD} stand for the variation size between actual value and the return value of linear, which are expected as smaller as possible. Thus, taking linear correlation coefficients r and standard deviations r_{SD} into the account, the mechanism functions would be ensured.

From Table 4, it can be seen that the data of No.3 are better, the correlation coefficients r are greater and the standard deviations r_{SD} are relatively smaller. Therefore, three-dimensional diffusion model of Jander equation is the most probable mechanism function for the thermal decomposition of high iron gibbsite ore, and the integral form and differential form are $G(\alpha)=[1-(1-\alpha)^{1/3}]^2$ and $f(\alpha)=(3/2)(1-\alpha)^{2/3}[1-(1-\alpha)^{1/3}]^{-1}$, respectively. And the mechanism code is D3, which is different from the mechanism function of gibbsite [9,10].

3.3 Calculation of kinetics parameters

In Propescu method, according to Eq. (7), the plot of $\ln[\beta/(T_n-T_m)]$ versus $1/T_\xi$ leads to a straight line,

Table 2 Typical kinetics mechanism functions

No.	Name of equation	Mechanism code	$G(\alpha)$	$f(\alpha)$
1	Two dimension (Valensi−Barrer)	D2	$\alpha+(1-\alpha)\ln(1-\alpha)$	$[-\ln(1-\alpha)]^{-1}$
2	Two dimension (Jander)	D8	$[1-(1-\alpha)^{1/2}]^2$	$(1-\alpha)^{1/2}[1-(1-\alpha)^{1/2}]^{-1}$
3	Three dimension (Jander)	D3	$[1-(1-\alpha)^{1/3}]^2$	$(3/2)(1-\alpha)^{2/3}[1-(1-\alpha)^{1/3}]^{-1}$
4	Ginstling−Brounshtein	D4	$1-(2/3)\alpha-(1-\alpha)^{2/3}$	$(3/2)[(1-\alpha)^{-1/3}-1]^{-1}$
5	Zhuralev−Lesokin−Tempelman	−	$[(1-\alpha)^{-1/3}-1]^2$	$(3/2)(1-\alpha)^{4/3}[(1-\alpha)^{-1/3}-1]^{-1}$
6	Avrami−Erofeev	−	$[-\ln(1-\alpha)]^{3/2}$	$(2/3)(1-\alpha)[-\ln(1-\alpha)]^{-2}$
7	Avrami−Erofeev	AE2	$[-\ln(1-\alpha)]^2$	$(1/2)(1-\alpha)[-\ln(1-\alpha)]^{-1}$
8	Reaction order	F2	$(1-\alpha)^{-1}$	$(1-\alpha)^2$
9	Reaction order	F2	$(1-\alpha)^{-1}-1$	$(1-\alpha)^2$
10	Reaction order	F3	$(1-\alpha)^{-2}$	$(1/2)(1-\alpha)^3$

Table 3 Conversion degrees measured for given temperatures with different heating rates

T/K	Conversion degree			
	5 K/min	10 K/min	15 K/min	20 K/min
472.99	0.200	0.135	0.117	0.110
513.47	0.300	0.199	0.167	0.156
527.89	0.400	0.254	0.204	0.188
541.44	0.500	0.343	0.272	0.244
559.21	0.600	0.459	0.395	0.363
576.68	0.700	0.556	0.497	0.469

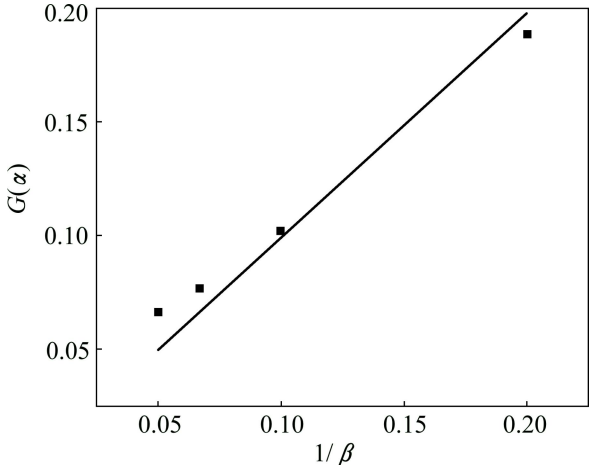

Fig. 6 Inferring schematic diagram of most probability mechanism function

whose slope is the value of the activation energy *E*. Values of the activation energy are thus computed, as well as the corresponding correlation coefficients. The values of the pre-exponential factor *A* are calculated from the values of the intercept of the plot. These results are listed in Tables 5 and 6. From Table 6, it can be seen that the largest correlation coefficient *r* is 0.95855. Thus, the most probable activation energy *E* and pre-exponential factor *A* are 75.36 kJ/mol and 1.51×10^5 s^{-1}, respectively.

3.4 Activation energy verification

Only the correct mechanism function corresponds to the right activation energy. Thus, the right activation energy also can test whether the mechanism function is correct [18,19].

In order to verify the thermal decomposition activation energy, Flynn−Wall−Ozawa (FWO) method was used to calculate the activation energy. FWO method was a typical method of iso-conversional method [22]. Compared with other methods, the method avoids the possibility of error, which resulted from the different kinetic mechanism function hypotheses, so the activation energy obtained by FWO method is more reasonable [23].

The equation of FWO method is as follows:

$$\ln\beta = \ln\left[\frac{AE}{RG(\alpha)}\right] - 2.315 - 0.4567\frac{E}{RT_P} \quad (8)$$

where T_P is the peak temperatures of corresponding DSC curves. In this work, the T_P is obtained from Fig. 3. Table 7 gives the activation energy *E* and correlation coefficients *r* of the endothermic peaks at different conversion degrees. As shown in Table 7, the average activation energy *E* is the average value of the activation energy of the endothermic peaks at different conversion degrees, and the value is of 79.44 kJ/mol, which relatively matches the value (75.36 kJ/mol) obtained by Popescu method. And the values satisfy the condition of $|(E_p-E_F)/E_p|=0.05\leq0.1$ [17]. Thus, the correctness of the thermal decomposition mechanism function is proved from the view of the activation energy.

Table 4 Linear fitting results of kinetic mechanism functions

No.	T_m= 513.47 K, T_n= 576.68 K		T_m= 472.99 K, T_n= 559.21 K		T_m= 472.99 K, T_n= 576.68 K		T_m= 513.47 K, T_n= 559.21 K		T_m= 527.89 K, T_n= 576.68 K	
	r	r_{SD}	*r*	r_{SD}	*r*	r_{SD}	*r*	r_{SD}	*r*	r_{SD}
1	0.96658	0.14667	0.99192	0.05002	0.97346	0.14160	0.98712	0.05547	0.94448	0.16773
2	0.98108	0.06578	0.99672	0.01822	0.98509	0.06279	0.99428	0.02134	0.96666	0.07806
3	0.99045	0.02469	0.99910	0.00485	0.99255	0.02328	0.99816	0.00619	0.98188	0.03063
4	0.97657	0.03062	0.99534	0.00922	0.98147	0.02936	0.99216	0.01057	0.95661	0.03687
5	0.98922	0.05620	0.98752	0.03211	0.98857	0.06029	0.98885	0.02793	0.99241	0.04372
6	0.97707	0.45438	0.98959	0.20770	0.98046	0.45622	0.98630	0.20735	0.96326	0.51139
7	0.99774	0.15591	0.99746	0.09696	0.99763	0.16851	0.99841	0.06953	0.99706	0.16250
8	0.98538	0.60718	0.98626	0.38927	0.98599	0.64904	0.98509	0.34898	0.97808	0.66309
9	0.98538	0.60718	0.98626	0.38927	0.98599	0.64904	0.98509	0.34898	0.97808	0.66309
10	0.98781	2.37656	0.99710	0.61605	0.98873	2.41045	0.99689	0.57178	0.98943	2.04269

Table 5 Temperatures measured for various conversion degrees on curves from Fig. 4

α	T/K			
	5 K/min	10 K/min	15 K/min	20 K/min
20	109.12	159.65	181.20	190.12
30	240.31	262.41	272.31	277.14
60	303.56	332.91	343.14	347.35
70	438.37	488.46	517.88	527.49

Table 6 Values of kinetic parameters for thermal decomposition of high iron gibbsite ore computed by Eq. (7)

$\alpha_n \cdots \alpha_m$	E/(kJ·mol^{-1})	A/s^{-1}	r
0.6⋯0.2	75.36	1.51×10^5	0.95855
0.7⋯0.2	70.96	0.55×10^5	0.94410
0.6⋯0.3	82.29	6.12×10^5	0.94099
0.7⋯0.3	79.28	2.86×10^5	0.92770

Table 7 Activation energy and correlation coefficients of endothermic peaks at different conversion degrees

α/%	Slope of fitting linear/s^{-1}	E/(kJ·mol^{-1})	r
5	−1.4856	27.04462	0.97947
10	−1.29149	23.51094	0.97238
15	−1.87902	34.20664	0.98555
20	−3.25723	59.29628	0.95434
25	−4.87652	88.77466	0.99440
30	−5.82102	105.96882	0.94906
35	−5.22749	95.16390	0.96942
40	−5.33129	97.05353	0.97426
45	−5.29419	96.37814	0.96763
50	−5.31285	96.71783	0.96137
55	−5.48681	99.88469	0.96140
60	−5.63175	102.52325	0.95406
65	−5.5847	101.66673	0.98885
70	−5.36018	97.57945	0.99317
75	−4.77032	86.84134	0.96092
80	−3.92239	71.40519	0.93298
85	−3.7822	68.85310	0.95371
90	−4.37043	79.56154	0.94868
95	−4.22443	76.90368	0.94902
Average activation energy		79.43865	

4 Conclusions

1) The thermal decomposition mechanism of high iron gibbsite ore follows the three dimensional diffusion model of Jander equation, whose integral form and differential form are $G(\alpha)=[1-(1-\alpha)^{1/3}]^2$ and $f(\alpha)=(3/2)(1-\alpha)^{2/3}[1-(1-\alpha)^{1/3}]^{-1}$, respectively.

2) The activation energy and pre-exponential factor for thermal decomposition kinetics of high iron gibbsite ore are 75.36 kJ/mol and 1.51×10^5 s^{-1}, respectively.

3) The correctness of the thermal decomposition mechanism function is proved from the view of the activation energy by the FWO method, and the Popescu method is a rational and reliable method for the research on the thermal decomposition mechanism of high iron gibbsite ore.

References

[1] MU Xin-he. Discussion on reasonable exploitation of bauxite mineral resources in China [J]. Mineral Resources and Geology, 2002, 16(5): 313−315. (in Chinese)

[2] LI Guang-hui, LIU Mu-dan, JIANG Tao, ZHOU Tai-hua, FAN Xiao-hui. Mineralogy characteristics and separation of aluminum and iron of high-aluminum iron ores [J]. Journal of Central South University: Science and Technology, 2009, 40(5): 1165−1171. (in Chinese)

[3] HU Wen-tao, WANG Hua-jun, LIU Xin-wei, SUN Chuan-yao. Effect of nonmetallic additives on iron grain grindability [J]. International Journal of Mineral Processing, 2014, 130(7): 108−113.

[4] LIU Zheng-gen, CHU Man-sheng, TANG Jue, HAN Yuan-ting, WU Xiang-long. Appropriate reduction and Fe−Al separation of high iron gibbsite [C]//SADLER B A. Light Metals 2013. San Antonio, TX: TMS, 2013: 223−227.

[5] PICKLES C A, CHAMBERS T L B, FORSTER J. A study of reduction and magnetic separation of iron from high iron bauxite ore [J]. Canadian Metallurgical Quarterly, 2012, 51(4): 424−433.

[6] SHI Guo-song, FANG Jue, YANG Gai-yan, GAO Yan-jia. Feasibility study of Guangxi high Fe bauxite sintering [J]. Journal of Hebei Polytechnic University: Natural Science Edition, 2011, 33(2): 11−13. (in Chinese)

[7] LI Yin-tai, BI Shi-wen, DUAN Zheng-yin, YANG Yi-hong, ZHANG Jing-dong. Discussion on the comprehensive utilization technology of high iron gibbsite ore in Guigang city Guangxi region [J]. Light Metals, 1992(9): 6−14. (in Chinese)

[8] ZHANG Zuo-liang, LI Qiang, ZOU Zong-shu. Reduction properties of high alumina iron ore cold bonded pellet with CO−H_2 mixture [J]. Ironmaking and Steelmaking, 2014, 41(8): 561−567.

[9] ZHU Bo-quan, FANG Bin-xiang, LI Xiang-cheng. Dehydration reaction and kinetic parameters of gibbsite [J]. Ceramics International, 2010, 36(8): 2493−2498.

[10] MACKENZIE K J D, TEMUUJIN J, OKADA K. Thermal decomposition of mechanically activated gibbsite [J]. Thermochimica Acta, 1999, 327(1−2): 103−108.

[11] AMIRPIRAN A, ANDREY V B, GORDON D I, IZTOK L, NICOLETA E M. A 1-D non-isothermal dynamic model for the thermal decomposition of a gibbsite particle [J]. Chemical Engineering Research and Design, 2013, 91(3): 485−496.

[12] AMIRPIRAN A, GORDON D I, ANDREY V B, IZTOK L, NICOLETA E M. A multi-stage, multi-reaction shrinking core model for self-inhibiting gas–solid reactions [J]. Advanced Powder Technology, 2013, 24(4): 728−736.

[13] POPESCU C. Integral method to analyze the kinetics of heterogeneous reactions under non-isothermal conditions a variant on the Ozawa−Flynn−Wall method [J]. Thermochimica Acta, 1996,

285(2): 309−323.
[14] ZHANG Jian-jun, REN Ning, BAI Ji-hai. Non-isothermal decomposition reaction kinetics of the magnesium oxalate dihydrate [J]. Chinese Journal of Chemistry, 2006, 24(3): 360−364.
[15] GAO Zhen-xin, HE Zhong-yang, ZHENG Xiao-ping, FU Qing-hua, SHI Xu-bo. Phase transformation and morphology of Bayer-gibbsite during heating [J]. Journal of the Chinese Ceramic Society, 2008, 36(S1): 117−123. (in Chinese)
[16] LIU Xue-fei, WANG Qing-fei, ZHANG Qi-zuan, ZHOU Fang, GAO Bang-fei, XU Hao. Thermal analysis of core of the ore body X in the Xinxu bauxite deposit, Jinxi county, Guangxi region [J]. Journal of Mineralogy and Petrology. 2008, 28(4): 53−59. (in Chinese)
[17] HU Rong-zu. Thermal analysis kinetics [M]. 2nd ed. Beijing: Science Press, 2008. (in Chinese)
[18] DICKINSON C F, HEAL G R. A review of the ICATC kinetics project, 2000 part 1: Isothermal results [J]. Thermochimica Acta, 2009, 494(1−2): 1−14.
[19] ZHANG Kun, LIN Shao-kun, LIN Mu-liang. Introduction to a new method for thermal analysis kinetics multivariate non-linear regression and its application [J]. Modern Scientific Instruments, 2002(5): 15−18. (in Chinese)
[20] CRADO J M, MDEK J, ORTEG A. Applicability of the master plots in kinetic analysis of non-isothermal data [J]. Thermochimica Acta, 1989, 147(2): 377−385.
[21] LIU Zhong-suo, WANG Qi, ZOU Zong-shu, TAN Guang-lei. Popescu method used for study on reaction mechanism of carbon gasification with CO_2 [J]. Research on Iron & Steel. 2011, 39(6): 12−17. (in Chinese)
[22] OZAWA T. A new method of analyzing thermogravimetric data [J]. Bulletin of the Chemical Society of Japan, 1965, 38(11): 1881−1886.
[23] ZHANG Xiang-hui, HE Chuan, WANG Ling, LIU Jing, DENG Miao, FENG Qian. Non-isothermal kinetic analysis of thermal dehydration of $La_2(CO_3)_3{\cdot}3.4H_2O$ in air [J]. Transactions of Nonferrous Metals Society of China, 2014, 24(10): 3378−3385.

基于 Popescu 法的高铁三水铝土矿非等温热分解动力学

柳政根[1]，王 峥[1]，唐 珏[1]，王宏涛[1]，龙红明[2]

1. 东北大学 材料与冶金学院，沈阳 110819；
2. 安徽工业大学 冶金工程学院，马鞍山 243002

摘 要：在非等温条件下研究高铁三水铝土矿的热分解动力学。利用 Pcpescu 法分析高铁三水铝土矿的热分解反应机理。结果表明，Jander 方程的三维扩散模型是高铁三水铝土矿热分解反应的最概然机理函数，函数机理代码为 D3。由 Popescu 法得到的高铁三水铝土矿热分解活化能和指前因子分别为 75.36 kJ/mol 和 1.51×10^5 s^{-1}。由等转化率方法求出的活化能验证了所求机理函数的正确性。Popescu 法是分析高铁三水铝土矿热分解反应机理较为合理和可靠的方法。

关键词：高铁三水铝土矿；热分解动力学；活化能；指前因子；Popescu 法

(Edited by Yun-bin HE)